

UC San Diego

UC San Diego Previously Published Works

Title

Live FRET-FLIM Imaging to Study Metabotropic Signaling via the NMDA Receptor

Permalink

<https://escholarship.org/uc/item/8cx1t5zq>

ISBN

9781071637418

Authors

Manikkoth, Mehreen

Dore, Kim

Publication Date

2024

DOI

10.1007/978-1-0716-3742-5_4

Copyright Information

This work is made available under the terms of a Creative Commons Attribution License, available at

<https://creativecommons.org/licenses/by/4.0/>

Peer reviewed



Live FRET-FLIM Imaging to Study Metabotropic Signaling via the NMDA Receptor

Mehreen Manikoth and Kim Dore

Abstract

Until recently, NMDA receptor (NMDAR) functions have been attributed to its ability to conduct calcium ions. However, growing evidence demonstrates that the NMDAR can induce synaptic depression without ion flux, suggesting that it has a metabotropic function. Our results show that glutamate binding or elevated amounts of beta-amyloid can trigger a conformational change in the NMDAR c-terminal domain. We have shown previously that this movement affects interactions between the NMDAR and signaling molecules, which results in synaptic depression. Here, we describe in detail how to monitor conformational movement in the NMDAR and its interactions with associated signaling molecules using FRET-FLIM live imaging in primary hippocampal neurons. A method to selectively block the NMDAR metabotropic function will also be explained. These approaches could be directly used to test the effect of novel NMDAR binding compounds on the NMDAR intracellular conformation or to study signaling proteins implicated in ion-flux-independent synaptic depression. Moreover, one could adapt these procedures to study any kind of protein-protein interaction and its dynamics in living cells.

Key words Long-term depression, LTD, Ion-flux-independent, Fluorescence lifetime imaging, Protein-protein interactions, CaMKII, PP1, Two-photon live microscopy

1 Introduction

The NMDA receptor (NMDAR) has historically been classified as an ionotropic receptor, essential for the induction of long-term potentiation (LTP) and long-term depression (LTD) [1, 2]. Early studies into the correlation between NMDAR activation, LTD, and LTP found that both LTP and LTD caused a rise in intracellular Ca^{2+} levels and were blocked by an NMDAR antagonist [4, 5]. This led to a model where a large increase in cytoplasmic Ca^{2+} was assumed to cause LTP, while a small increase in cytoplasmic Ca^{2+} causes LTD. However, growing body of evidence indicates that NMDAR-dependent LTD can be induced, while NMDAR ion flux is blocked, suggesting that the NMDAR has a metabotropic function in addition to its recognized ionotropic function [8–12].

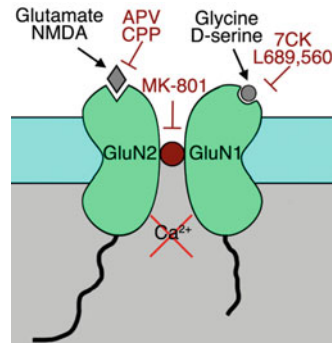


Fig. 1 Drugs affecting NMDARs. Glutamate and NMDA bind to GluN2 subunits to activate NMDARs. APV and CPP are competitive antagonists for this site and block NMDAR activation. MK-801 blocks ion flux by blocking open channels. Co-agonist binding (glycine, D-serine) happens on GluN1 subunits. 7CK and L689,560 are antagonists for this site and block NMDAR activation and ion flux

Interestingly, the first experiments showing ion-flux-independent LTD were reported almost 30 years ago but were not really discussed [13, 14]. The first detailed study on the requirement of ion flux through the NMDAR for LTD came out in 2013 [11]. These slice electrophysiology experiments showed that low-frequency stimulation in the presence of two drugs that effectively block NMDAR currents (MK-801 or 7-chlorokynurenate (7CK)) produced the same level of synaptic depression as controls ([11]; see Fig. 1 for binding sites). The mechanism underlying NMDAR ion-flux-independent function was proposed to be due to a conformational change in NMDAR c-terminal domain [6]. To reveal this conformational movement, live fluorescence lifetime imaging microscopy (FLIM) was used to monitor fluorescence resonance energy transfer (FRET) between GluN1 subunits tagged with GFP and mCherry [6]. These experiments demonstrated that binding of NMDAR agonists (NMDA and glutamate) on the extracellular side is inducing a conformational change in the intracellular side of the NMDAR, its cytoplasmic domain (cd). This change in FRET efficiency was seen in the presence of the NMDAR antagonists 7CK and MK-801, indicating that the conformational change in the NMDARcd is ion-flux-independent [6]. Importantly, blocking NMDARcd movement using an antibody binding to GluN1 c-terminal domain completely blocked ion-flux-independent LTD, demonstrating the requirement of NMDARcd movement for this type of synaptic plasticity [8]. Furthermore, FRET-FLIM experiments showed that NMDARcd movement triggered changes in protein-protein interactions between GluN1 and the signaling proteins PP1 (protein phosphatase 1) and CaMKII (Ca^{2+} /calmodulin-dependent protein kinase II), possibly mediating synaptic depression [8]. Interestingly,

overexpression of the scaffolding protein PSD-95 (postsynaptic density protein-95), which binds to the NMDARcd, blocks NMDARcd conformational changes and ion-flux-independent LTD [15]. Since larger dendritic spines contain more PSD-95 and larger dendritic spines are more stable [16], the fact that PSD-95 overexpression blocks ion-flux-independent LTD could be one of the mechanisms implicated in preserving important dendritic spines. LTD is also correlated with shrinkage of dendritic spines, for which NMDAR activation is necessary [17]. Since ionotropic NMDAR function is not necessary for LTD, a study by Stein et al. [18] investigated whether ionotropic NMDAR function was required to induce dendritic spine shrinkage. While blocking Ca^{2+} influx through the NMDAR using 7CK had no significant effect on spine shrinkage, the NMDAR antagonist CPP (*see* Fig. 1 for binding sites) prevented spine shrinkage, confirming the necessity of agonist binding for LTD and spine shrinkage [18].

Amyloid-beta ($\text{A}\beta$), a peptide implicated in Alzheimer's disease, causes synaptic depression that is also mediated by the ion-flux-independent function of the NMDAR [19–22]. Acute application of $\text{A}\beta$ oligomers to hippocampal neurons resulted in synaptic depression within 10 min [22]. Synaptic depression was blocked by APV (2-amino-5-phosphonovaleric acid) but not MK-801, indicating that this effect is mediated by the NMDAR ion-flux-independent function [22]. Similarly, paired recordings in hippocampal slices showed that MK-801 did not block synaptic depression caused by viral expression of CT100, a fragment of APP (amyloid precursor protein) [21]. The same *in vitro* model of Alzheimer's disease, CT100 expression, triggered a conformational change in the NMDARcd that was blocked by elevated PSD-95 [20]. Spine elimination in cultures made from AD model mice was blocked in the presence of the NMDAR glutamate binding site antagonist APV but was unaffected by the channel pore blockers MK-801 and memantine [19]. Together, these findings strongly implicate ion-flux-independent NMDAR signaling in the etiology of Alzheimer's disease. Interestingly, the NMDAR ion-flux-independent function is also implicated in excitotoxicity [23] and schizophrenia [24], indicating that this form of NMDAR signaling has many roles and that research on this topic is only beginning.

In this chapter, we will first explain the rationale supporting the use of FLIM to measure FRET (Subheading 1.1), then describe the use of FRET-FLIM to monitor conformational movement in the NMDARcd (Subheading 1.2), and study interactions between the NMDAR and signaling proteins (Subheading 1.3). Next, we provide a descriptive list of all materials needed for preparing primary neuronal cultures (Subheading 2.1), two-photon FLIM (Subheading 2.2), and electrophysiology (Subheading 2.3). This “Materials” section is followed by the “Methods” section which provides step-by-step protocols for primary hippocampal culture preparation

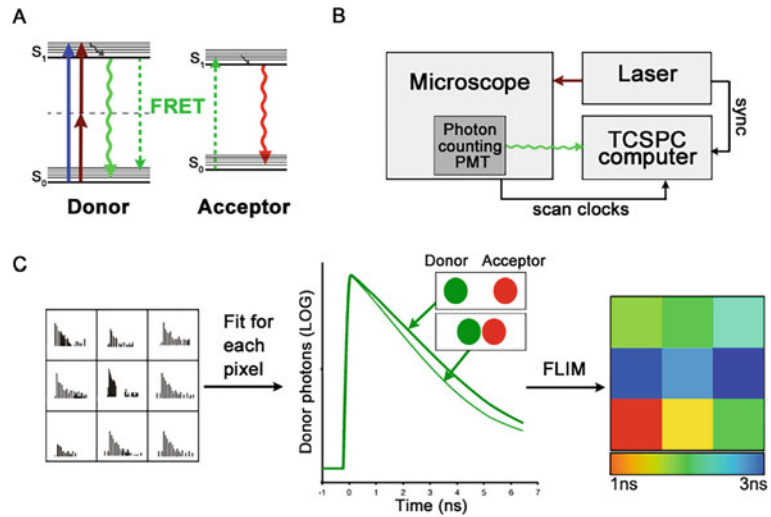


Fig. 2 Use of FLIM to measure FRET. (a) Jablonski diagram of FRET donor and acceptor energy levels. After excitation by a one-photon (blue arrow) or two-photon (brown arrows) laser, the FRET donor can return to ground state by emitting a photon (green arrow) or by transferring its energy to a nearby acceptor (dashed green arrows). (b) Wiring diagram of a typical FLIM system. (c) TCSPC records fluorescence decay curves for each pixel of an image. By fitting these curves, the fluorescence lifetime of the FRET donor, which becomes shorter with increased proximity of the FRET acceptor, can be assessed. The FLIM image is then color coded according to the FRET donor lifetime at each pixel (color scale shown below image). (Adapted from [7])

(Subheading 3.1), expression of the NMDAR FRET constructs (Subheading 3.2), live time-lapse FLIM (Subheading 3.3), antibody infusion to block NMDARcd movement (Subheading 3.4), and data analysis (Subheading 3.5). Finally, we conclude by discussing limitations of the technique (Subheading 4.1), other applications of FRET-FLIM in neuroscience, and future perspectives (Subheading 4.2).

1.1 Fluorescence Lifetime Imaging (FLIM) to Measure Förster Resonance Energy Transfer (FRET)

Fluorescence can be defined as the ability of certain chemicals, called fluorophores, to emit visible light after absorbing light of higher energy. For example, GFP is excited at 480–500 nm (or 900–950 nm if using two-photon excitation) and emits fluorescence from about 500 to 550 nm, peaking at 511 nm (Fig. 2a). FLIM measures fluorescence lifetime, which can be defined as the average amount of time a fluorescent molecule remains in its excited state, by measuring the time delay between laser excitation and photon arrival time for each pixel of an image (Fig. 2). This approach, time-correlated single-photon counting (TCSPC, [25]), is the most commonly used approach for FLIM (Fig. 2b). Briefly, the excitation laser is scanned onto the sample, and the fluorescence is detected with a photon-counting PMT (this type of PMT is

required for FLIM). Then, the TCSPC computer integrates three signals at the same time: (1) the SYNC signal that comes from each laser excitation pulse, (2) the arrival time of each photon detected by the PMT, and (3) the scan clocks coming from the microscope (Fig. 2b). For each pixel, a fluorescence decay curve is built, and fluorescence lifetimes are calculated and color-coded to generate a FLIM image (Fig. 2c). This FLIM image contains both intensity (number of photons collected for each pixel) and fluorescence lifetime information (extracted from the fluorescence decay curve).

Fluorescence lifetime depends on the fluorophore structure, so each dye or fluorescent protein has its own fluorescence lifetime [26]. This intrinsic fluorescence lifetime is also affected by the physiological and chemical environment of the fluorophore. For example, fluorescence lifetime of all fluorophores is affected by temperature, index of refraction, and the proximity of a suitable FRET acceptor [26]. Moreover, some fluorophores are sensitive to specific ions and can be used as sensors. For example, the fluorescence lifetime of the dye MQAE (N-(ethoxycarbonylmethyl)-6-methoxyquinolinium bromide) is sensitive to chloride concentration and can be used as a chloride sensor in live preparations [27]. Importantly, the fluorescence lifetime extracted from the fluorescence decay curve (Fig. 2c) will not change if the amplitude of this decay curve changes [26]. This means that the fluorescence lifetime is not affected by fluorophore concentration, the power of the excitation laser or the voltage applied to the detection PMT. This is especially useful for biological applications when fluorescent proteins like GluN1-GFP (FRET donor used in this protocol) are expressed in cells, resulting in varying levels of expression [28]. Because photobleaching results in decreases in fluorescence intensity, this property of FLIM also makes this imaging approach less sensitive to photobleaching. Most intensity-based sensors, like Oregon green BAPTA (OGB), also undergo fluorescence lifetime changes upon activation of the associated molecule (binding of calcium ions to BAPTA in this case), and because FLIM is much less sensitive to photobleaching, this can result in more accurate measurements (*see* Fig. S5 in [6]).

Förster resonance energy transfer (FRET) is a non-radiative energy transfer mechanism between two fluorescent molecules. There are two main requirements for successful FRET. First, the fluorescence emission of the FRET donor must overlap with the FRET acceptor absorption spectrum, and, second, these fluorescent molecules must be no more than ~10 nm apart from each other [26]. This spatial requirement of FRET is very sensitive to the distance and orientation of the interacting fluorophores; it can thus be used as a “molecular ruler” to assess protein structure [29] or to monitor subtle conformational changes [6]. FRET can be measured by acquiring a series of images in different combinations of excitation and emission channels or by photobleaching of the

FRET acceptor. However, while these methods work well with FRET sensors (in which the FRET donor and acceptor are linked together and expressed as a single construct), they are generally not well suited for intermolecular FRET measurements used to study protein-protein interactions [28, 30, 31]. As explained above, fluorescence lifetime is not affected by intensity (e.g., level of expression of fluorescent proteins) but is sensitive to FRET. Specifically, the FRET acceptor absorbs the energy released by the FRET donor (through dipole-dipole interactions), which adds an additional route for the donor fluorophore to return to ground state (Fig. 2a). This process makes the fluorescence lifetime of the FRET donor proportionally shorter and allows for precise FRET measurements (Fig. 2a, c). FRET-FLIM is thus the best method to measure protein-protein interactions in living cells [28].

1.2 FRET-FLIM to Monitor Conformational Movement in the NMDARcd

FRET-FLIM has been used to measure the intracellular conformation of the NMDAR and how it is affected by neurotransmitter binding [6]. The GluN1 subunit of the NMDAR is an obligatory subunit (there are two GluN1 subunits in every NMDAR) and has the shortest intracellular domain. Recombinant GluN1 subunits of the NMDAR were thus tagged with GFP or mCherry at their carboxyl(c)-terminus (Fig. 3a) and co-expressed into primary cultured hippocampal neurons. Unlabeled GluN2B was also expressed at the same time in order to form complete NMDARs and thus maximize synaptic targeting. The decrease in fluorescence lifetime seen when GluN1-GFP and GluN1-mCherry were co-expressed corresponds to an average distance of 8.3 nm in dendritic spines, which is still (to our knowledge) the only structural information available about the intracellular domain of the NMDAR [6]. Careful control experiments indicated that the variation in GluN1-GFP lifetime in neurons expressing GluN1-GFP/

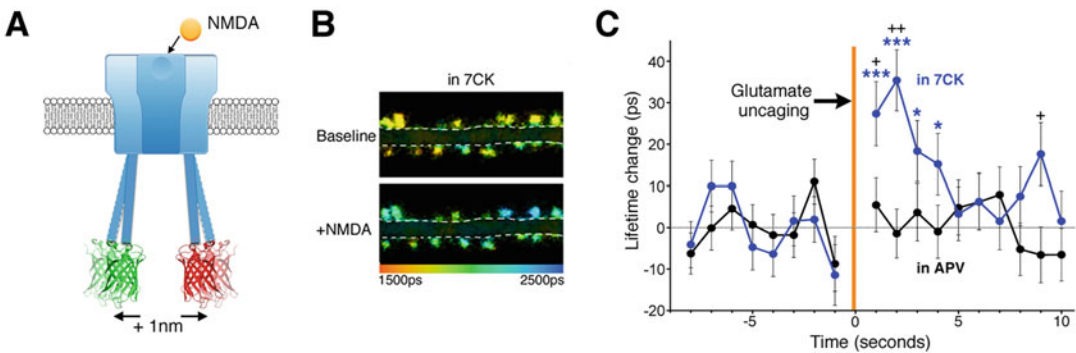


Fig. 3 Measurement of a conformational change in the NMDARcd using FRET-FLIM. (a) GluN1 subunits tagged at their c-terminus with GFP or mCherry. (b) NMDA application in the presence of 7CK triggers an increase in GluN1-GFP lifetime. (c) Glutamate uncaging shown that the lifetime increase is transient and remains only while the agonist is bound to the receptor. (From [6])

GluN1-mCherry/GluN2B is due to biological differences among spines, as well as between spines and dendrites, producing different NMDARcd conformations, rather than noise in lifetime measurements [6]. Moreover, a number of different observations confirmed that the measured FRET was caused by intrareceptor FRET between GluN1-GFP and GluN1-mCherry on individual NMDARs and not interreceptor FRET between different NMDARs (*see* [6] for more details). Bath application of glutamate or NMDA in the presence of MK-801 or 7CK, but not APV, produced a transient change in FRET consistent with conformational movement of the NMDAR cytoplasmic domain (Fig. 3b). Glutamate uncaging and fast fluorescence lifetime measurements confirmed that the conformational change persists only while glutamate is bound to the receptor (Fig. 3c).

Importantly, some of these findings were replicated by Ferreira et al., who used the same approach to investigate conformational changes in the NMDAR caused by the application of different agonists [10]. They found that stimulating the NMDAR with D-serine decreased the lifetime of GluN1-GFP, indicating that this co-agonist caused the GluN1 subunits to move closer together [10]. Stimulating with glycine failed to produce the same effect, indicating differences in the conformational changes of the NMDAR in response to varying agonists. This study independently confirmed that NMDA application results in conformational changes in the NMDARcd [10]. They used the same approach but different FRET-FLIM instrumentation, demonstrating the replicability of our findings [6]. This protocol could be used to test the effect of other molecules that can bind NMDARs, such as the allosteric modulators UBP684 and pregnenolone sulfate, that elicited different conformational changes in the NMDARcd [32]. To test if ligand-driven NMDARcd movement is required for ion-flux-independent LTD, neurons were infused with a patch pipette containing an antibody targeting the c-terminal domain of GluN1 (or a control antibody), which would be expected to bind, and immobilize, two nearby GluN1 c-tails. This approach did block the ligand-driven FRET change as well as chemically induced LTD in the presence of 7CK, suggesting that the conformational change in the NMDARcd is required for the induction of ion-flux-independent LTD [8].

1.3 FRET-FLIM to Study Interactions Between the NMDAR and Signaling Proteins

FRET-FLIM can also be used to visualize dynamic interactions between different proteins. In this section, we will describe experiments in which FRET-FLIM was used to study the interaction between the NMDAR and other signaling proteins and how these interactions are regulated during synaptic plasticity. PSD-95 is a scaffolding protein that directly interacts with and stabilizes NMDARs at synapses [33]. Expressing the same FRET donor as in the NMDARcd studies, GluN1-GFP and PSD-95-mCherry as a

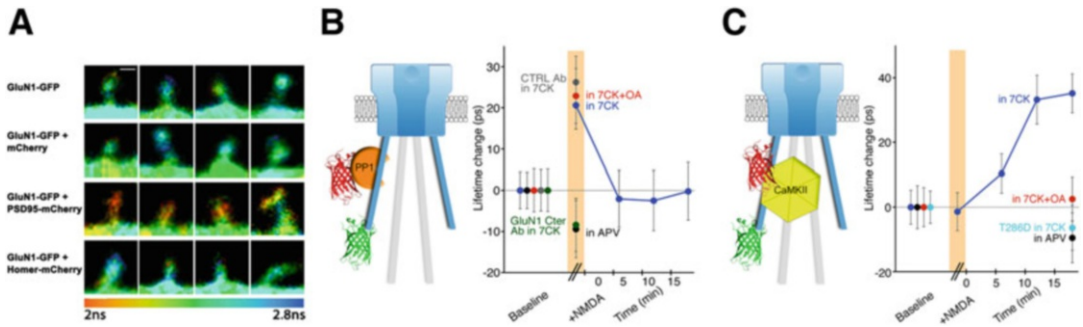


Fig. 4 Measurement of NMDAR interactions with PSD-95, PP1, and CaMKII with FRET-FLIM. **(a)** Expression of PSD-95-mCherry but not Homer-mCherry leads to a significant decrease in GluN1-GFP fluorescence lifetime. (From [3]). **(b)** NMDA application transiently reduces the interaction between GluN1 and PP1. (Modified from [8]). **(c)** NMDA application also reduces the interaction between GluN1 and CaMKII, but this occurs in a delayed fashion. (Modified from [8])

FRET acceptor resulted in significant FRET in the dendritic spines of hippocampal neurons, as measured by marked decrease in GluN1-GFP fluorescence lifetime [3]. This decrease in lifetime was not seen when GluN1-GFP was co-expressed with mCherry or Homer-mCherry, indicating that the proximity of proteins in the postsynaptic density was not sufficient to produce FRET (Fig. 4a). Chemical LTP stimulation resulted in a decrease in the interaction between PSD-95 and the NMDAR and was correlated with an increase in dendritic spine volume. Treating neurons with an inhibitor of the protease calpain fully blocked the NMDAR activation-dependent dissociation between PSD-95 and the NMDARs and structural plasticity, suggesting that the regulation of the NMDAR/PSD-95 interaction is important for LTP [3].

Protein phosphatase 1 (PP1) is required for LTD and binds to the NMDAR complex [34, 35]. FRET between PP1-mCherry and GluN1-GFP was measured in basal conditions and was transiently reduced upon NMDA application [8]. This change in FRET was seen as an increase in GluN1-GFP lifetime and could reveal a shift in PP1 location or orientation in respect to GluN1 c-terminus (Fig. 4b). Okadaic acid, a PP1 inhibitor, did not affect this FRET change, indicating that PP1 activity is not necessary for this process. However, it was found to be dependent on NMDARcd conformational movement as infusion of the GluN1c-terminal antibody blocked the change in FRET between GluN1 and PP1 [8]. Interestingly, overexpression of A β also affected FRET between PP1-mCherry and GluN1-GFP, leading to an increase in PP1 activity [20].

Calcium/calmodulin-dependent protein kinase II (CaMKII) is implicated in both LTP [36, 37] and LTD [13, 38], binds to the NMDAR [39], and is a target protein for PP1. By monitoring FRET between GluN1-GFP and CaMKII-mCherry, a delayed

decrease in the NMDAR-CaMKII interaction was observed during ion-flux-independent LTD [8], Fig. 4c. Interestingly PP1 inhibition (with okadaic acid) blocked this increase in GFP lifetime, suggesting that PP1 would dephosphorylate CaMKII. This was confirmed using a CaMKII mutant that cannot be dephosphorylated at Thr-286 (CaMKII-T286D-mCherry), suggesting that dephosphorylation of Thr-286 is necessary to modify the NMDAR-CaMKII interaction [8].

Overall, these experiments demonstrate that FRET-FLIM is a very useful tool to study NMDAR interactions and signaling during synaptic plasticity. Further investigation using this approach might reveal important molecular mechanisms involved in learning and memory as well as neurodegeneration and synaptic dysfunction.

2 Materials

2.1 Primary Hippocampal Neurons

1. P0-P2 rat or mouse pups (one to two pups are sufficient to make a full 12-well plate of primary hippocampal neurons).
2. Dissection media (in mM: 82 Na₂SO₄, 30 K₂SO₄, 5.8 MgCl₂, 0.25 CaCl₂, 8 glucose, 1 HEPES buffer; 2% phenol red solution).
3. Dissociation media (dissection media supplemented with 2 mM L-cysteine hydrochloride, ~10–20 units papain (P4762, Sigma) (*see Note 1*), pH adjusted to ~7.4).
4. Low-magnification dissection microscope (Zeiss, Stemi 2000).
5. P1000 pipette (Gilson).
6. DNaseI (195 U/ul, Invitrogen).
7. 70 µm cell strainer (Corning).
8. Sterile 15 mL and 50 mL falcon tubes (Genesee Scientific).
9. Centrifuge (Eppendorf, Beckmann, or any centrifuge that can handle 50 mL tubes).
10. Plating media (Neurobasal-A (Gibco), 10% FBS, 0.5% Pen/Strep, and 0.25% Glutamax).
11. Reduced serum media (Neurobasal-A (Gibco), 5% FBS, 0.5% Pen/Strep, and 0.25% Glutamax).
12. Neuronal culture media (Neurobasal-A (Gibco), 2% B27 (Gibco), 0.5% Pen/Strep, and 0.25% Glutamax).
13. 18 mm PDL-coated glass coverslips (Neuvitro).
14. CO₂ incubator (Binder or equivalent), set at 37 °C and 5% CO₂.
15. Lipofectamine 2000 (Invitrogen).

16. GluN1-GFP, GluN2B, and GluN1-mCherry plasmid DNA. To study the NMDAR interactions with PSD-95, PP1, and CaMKII or other proteins, replace the GluN1-mCherry construct with the desired construct tagged with a red fluorescent protein. All these constructs are available upon request.
17. Opti-MEM (Gibco).

2.2 Two-Photon Fluorescence Lifetime Microscope

Hardware:

1. Multiphoton microscope (Scientifica Multiphoton SliceScope).
 - (a) Must include an epifluorescence system to find and identify suitable neurons expressing the proteins of interest.
 - (b) A water immersion objective with NA >1 is required.
2. Ultrashort pulsed laser (Coherent Chameleon Ultra II) (*see Note 2*).
3. Hybrid photon-counting PMT detector (Becker-Hickl HPM-100-40).
4. Time-correlated single-photon counting module (Becker-Hickl SPC-150) (*see Note 3*).

Software:

5. Laser scanning control software (ScanImage 3.8).
6. TCSPC software (Becker-Hickl SPCM).
7. Analysis software (Becker-Hickl SPCImage).

Imaging solution:

8. 0.87× Hank's Balanced Salt Solution (HBSS), 10 mM HEPES, 5 mM MgCl₂, and 0.6 mM CaCl₂. Glucose 2 mM (*see Note 4*).

2.3 Electro- physiology Equipment to Infuse Antibodies into Neurons

1. Axopatch 1D Amplifier from Axon Instruments (now Molecular devices) with headstage. Any recent version of this amplifier will also work.
2. Sutter micromanipulator.
3. 2 mm diameter glass pipettes with a resistance of 3–5 MΩ.
4. Oscilloscope (Tektronix, model TDS 3012B); any comparable oscilloscope will also work.
5. Optical table (Newport).

3 Methods

3.1 Preparation of Primary Hippocampal Neurons

1. Remove brain from P0-P2 mouse or rat pups and place in ice-cold dissection media.
2. Dissect hippocampi in a 60 mm petri dish under a low-magnification dissection microscope.

3. Cut hippocampi into fine pieces with a scalpel.
4. Resuspend tissue in dissociation media.
5. Incubate at 37 °C with gentle rocking for 15 min.
6. Add 1 μ L or 195U of DNaseI.
7. Use a P1000 pipette to further dissociate hippocampal tissue; about 10–20 ups and downs should be sufficient. No pieces of tissue should be visible after this process; the solution should appear cloudy.
8. Filter neurons through a 70 μ m cell strainer to remove undissociated tissue.
9. Spin at $3000 \times g$ at room temperature for 5 min.
10. Resuspend neurons in plating media and count neurons.
11. Place a 300 μ L drop of neurons at 10^6 cells/mL in the center of an 18 mm PDL-coated glass coverslip. If using smaller coverslips, scale accordingly.
12. Place neurons in a CO₂ incubator for 1.5–2 h.
13. For each individual well: Gently add 1 mL of plating media, remove it using a Pasteur pipette connected to vacuum, and add 2 mL of reduced serum media (Subheading 2.1, item 10).
14. Replace half the media with neuronal culture media (Subheading 2.1, item 11) on day 2, day 5, and for every 2–4 days.
15. Replace media more frequently (every other day) for older cultures.
16. Issues with low density and unhealthy cultures are most often due to incomplete dissociation, bad reagents (papain and coverslips are especially critical), and/or too old pups. For best results, use P0 pups, freshly dissolved papain, and tested coverslips.

3.2 Expression of Fluorescently Tagged NMDAR Subunits and/or Other NMDAR Interacting Proteins

1. For better transfection efficacy, use 6–7 DIV (days in vitro) neurons and Lipofectamine 2000.
2. All numbers in this section assume the use of 18 mm coverslips in a 12-well plate.
3. Perform all following steps in a biosafety cabinet to maintain sterility of the materials used.
4. In a microcentrifuge tube, add 4 μ L of Lipofectamine 2000 per coverslip to be transfected.
5. Dilute Lipofectamine with 100 μ L of Opti-MEM per coverslip.
6. Prepare DNA mixes: As a general rule of thumb, use a maximum of 2 μ g of total DNA per coverslip and a 1:2 (or 1:3) ratio of FRET donor to FRET acceptor. For looking at the NMDAR conformation, use 0.33 μ g of GluN1-GFP DNA, 0.66 μ g of

GluN1-mCherry DNA, and 1 μg of GluN2B DNA. If the FRET acceptor is not an NMDAR subunit, the amount of GluN2B DNA should be scaled down. Dilute DNA in 100 μL of Opti-MEM per coverslip.

7. Add 100 μL of diluted Lipofectamine per coverslip to the DNA solutions.
8. Remove half of the existing media from each well and add 200 μL of transfection mix.
9. Incubate the cells at 37 $^{\circ}\text{C}$.
10. After 4 h of incubation, place coverslips in a new plate containing 2 mL of neuronal culture media per well along with 100 μM APV to prevent excitotoxicity.
11. Issues with low transfection efficacy can be due to contaminated DNA or cultures that are too dense or unhealthy.

3.3 Live Fluorescence Lifetime Imaging

1. Warm imaging solution to 37 $^{\circ}\text{C}$.
2. Add 7CK (final concentration 100 μM), L-689,560 (final concentration 10 μM), or MK-801 (final concentration 100 μM) to block NMDAR ion flux.
3. Set up perfusion at a rate of one drop per second.
4. Set up the coverslip in the perfusion chamber.
5. Use epifluorescence to visualize GFP and mCherry. For example, we use a 470 nm LED for GFP and a 550 nm LED for mCherry.
6. Scan the coverslip to find neurons with good GluN1-GFP expression in dendritic spines. Make sure the neuron also expresses GluN1-mCherry or another protein tagged with a red fluorescent protein (the FRET acceptor). Use Scientifica LinLab2 to record the coordinates of each neuron to be imaged (*see Note 5*).
7. Focus on a specific dendrite to image. Ideally choose a branch point on the dendrites to maximize the number of dendritic spines within one image.
8. Close the epifluorescence light source and switch to the two-photon mode.
9. Use ScanImage version 3.8.1 to capture images. Configure the settings to ensure a standard pixel size (80 nm; all 512 \times 512 pixels), across all images. Set the zoom to 4 and click “Focus” on the ScanImage interface.
10. Open Single Photon Counter Version 9.84 (SPCM). Ensure that the SYNC signal from the laser (*see Fig. 1b*) corresponds to the expected repetition rate.
11. Close the hood over the microscope setup to minimize external light interference with imaging.

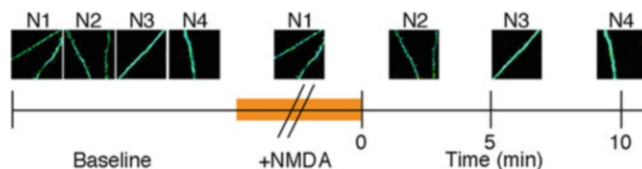


Fig. 5 Imaging protocol used for time course imaging experiment. Baseline images were acquired from different neurons (N) for each time point. Post-baseline images were then captured in the presence of NMDA (orange bar/“+NMDA”) or after NMDA washout. This method can be adapted to look at longer time scales. (From [6])

12. Enable outputs using the Detector Control Card DCC-100/110 version 2.40.
13. Set FLIM acquisition time to ~120 s per image and pixel dwell time to 3.2 μs (*see Note 6*). Open the shutter for the laser and click “Start!” on the SPCM interface to begin acquiring the image. While acquiring, gently shift the focus to ensure the dendrites and spines are clearly visible. One might set up a z-stack in ScanImage instead; in our experience, this manual approach yielded better quality images (*see Note 7*).
14. If neurons are to be stimulated with NMDA, for example, switch perfusion to a second solution containing 25 μM NMDA. Acquire a second picture after about 2 min to allow for the second solution to reach the neurons. After 5 min of NMDA stimulation, switch back to the other solution. In our hands, this is ideal to induce LTD. Figure 5 describes a method to acquire a time course to look at the effect of stimulation in up to four different neurons.
15. Issues with movement of the coverslip are most likely due to improper perfusion adjustment; perfusion speed must be the same for the two different solutions, not be too fast, and not cause any visible movement when entering the sample chamber.
16. Issues with low signal can be due to misalignment of the excitation laser; make sure to routinely check power under the objective; in our system, 2–5 mW at 930 nm leads to good images.

3.4 Infusion of an Antibody Binding to GluN1 C-terminal Domain via a Patch Pipette to Block NMDAR Metabotropic Function

1. If one wants to block the ion-flux-independent function of the NMDAR, a GluN1-c-terminal antibody can be used.
2. The antibody that was used in the original publication [6], MAB1570, is no longer available. However, another antibody, raised against the exact same peptide sequence, located at the end of the C2 cassette of rat GluN1 (amino acids 909-938 [LQNQKDTVLPRAIEREEGQLQLCSRHRRES]) is available from Millipore Sigma (AB9864).

3. Use a cesium-based internal solution (containing in mM: 115 cesium methanesulfonate, 20 CsCl, 10 HEPES, 2.5 MgCl₂, 4 Na₂ATP, 0.4 Na₃GTP, 10 sodium phosphocreatine, 0.6 EGTA, and 0.1 spermine, pH 7.25), and add in the GluN1 C-terminal antibody or the control antibody (GAR-AF647) and some water to adjust the osmolality (to ~290 mOsm/kg) to compensate for the higher osmolality of the antibody solution. Since there is no concentration provided for AB9864, we tested the following dilution, 296 uL internal solution, 2 uL water, and 2 uL AB9864, and confirmed that this antibody dilution blocked NMDARcd movement.
4. When a suitable neuron is identified under the FLIM microscope using epifluorescence, fill a glass recording pipette with the internal solution supplemented with the AB9864 antibody, put it on the headstage, and approach the pipette onto the neuron using the micromanipulator.
5. Use the amplifier to generate a seal test (using 0.2 mV oscillations) and the oscilloscope to see it (connect to scaled output on the amplifier, use a horizontal scale of 0.5 ms/division and a vertical scale corresponding to 0.5–1 V). After getting a good seal, obtain whole-cell access and clamp the cell to –60 mV. Let the antibody diffuse into the neuron for 5 min.
6. Remove the patch pipette. It is crucial to be very gentle at this step; the neuron must remain alive and healthy for imaging. Proceed with imaging as described in Subheading 3.3, step 7 to 14.

3.5 Data Analysis

1. Export data from SPCM into SPCImage version 8.3.
2. Find optimal fitting conditions to calculate GluN1-GFP fluorescence lifetime using your setup. In our experiments, single exponential fitting was used; other parameters were not fixed. The same calculated IRF (instrumental response function) was used for all images in a dataset.
3. Use the options tab to adjust image intensity so that spines are clearly visible. If desired, contrast can be adjusted to remove background noise in the image. Binning can be used to permit fluorescence lifetime calculations in images with less intensity.
4. Set the color range to be continuous between 1500 and 2500 ps.
5. Calculate the decay matrix for your image. Save the file and export the color-coded values, chi-square values, pixel intensities, and color-coded image to the hard drive.
6. Select the spines and their corresponding dendrites and record the spine lifetime, spine intensity, spine size, and dendrite lifetime for each region of interest (ROI) selected. Export this information into excel for further analysis (*see Note 8*).

7. In excel, spines were excluded from analysis according to the following criteria: (1) total integrated intensity was <100 photons (without binning), (2) the intensity of the second measurement was less than 50% of the first measurement, and (3) spines with the highest 5% lifetimes in the baseline image (to find these, sort the fluorescence lifetimes and remove the spines that have the highest fluorescence lifetime; for 100 spines, the five spines with the highest lifetimes should be removed). For more information about the rationale behind data exclusion, please see the Supplementary information in Dore et al. [6]. Note that points 2 and 3 only apply to experiments where neurons are imaged twice.

4 Conclusions

4.1 Limitations

FRET-FLIM is a technique broadly applicable for studying protein-protein interactions in a variety of cell types. Visualizing these interactions allows for a more in-depth understanding of the molecular mechanisms behind common processes. However, its usefulness is limited by the size and nature of the proteins studied and the fluorescent tags used. To accurately determine the nature of the interactions between two proteins, each one must be fluorescently tagged. For most applications, this means that a fluorescent protein must be linked to the protein of interest. When doing so, it's important to make sure that this does not affect trafficking and/or function of the protein. This might require some trial and error especially for large proteins as the fluorescent tags must be within ~ 10 nm from each other for FRET to be accurately used as a measure of distance and interaction [26]. Additionally, the acquisition time for FRET-FLIM imaging is quite long. From our experience, it requires about 60–120 s to obtain 40 μm wide images of the highest quality and clarity in primary hippocampal neurons. This can be circumvented by using fluorescence lifetime decay curves rather than images (as seen in Fig. 3c), but this technique does not provide as much information. Alternatively, one can image smaller dendritic segments and/or optimize fluorescence lifetime determination as demonstrated by the Yasuda laboratory [40]. Importantly, some specific fluorescent tags are susceptible to alteration of their fluorescence lifetime due to homo-FRET. Homo-FRET, or energy migration, occurs when there is overlap between the emission and absorption spectra of a fluorescent molecule, resulting in energy being transferred between two identical molecules [41]. This can interfere with the measurement and calculation of FRET between the intended donor and acceptor fluorophores. Certain fluorophores, such as cyan fluorescent protein (CFP) and Cerulean, have been demonstrated to have issues with homo-FRET [41]. Another important parameter to consider is the effect of fixation on the fluorescence lifetime. Because it is sensitive

to the refraction index, fixation and mounting changes the fluorescence lifetime [42]. Consequently, samples must be prepared the same way to allow for quantitative comparison. Any studies using FRET-FLIM must take into careful consideration these limitations in order to get meaningful results.

4.2 Other Applications of FRET-FLIM in Neuroscience and Future Perspectives

In this book chapter, we described the use of FRET-FLIM to study the NMDAR conformation and its interactions with other signaling molecules implicated in synaptic plasticity (PSD-95, PP1, and CaMKII). This technique is being used more and more in neuroscience research, especially in the last 10 years. The Yasuda group has made very important contributions to this field, developing numerous sensors to monitor the activity of CaMKII [40], PKA [43], Ras [44], RhoA [45], and CREB [46], to name a few. Several labs are now even using these sensors and FRET-FLIM in living animals [46–48], demonstrating the tremendous potential of this approach. Although there are less publications reporting applications of FRET-FLIM to study intermolecular interactions in neurons, here are a few interesting examples. FRET-FLIM was used to study SNARE protein complexes assembly in presynaptic terminals during exocytosis [49] and during A β exposure [50]. Others have used it to measure the dynamics of the APP-BACE1 interaction [51] or to study the interaction between presenilin 1 and alpha-synuclein [52]. Interestingly, FRET-FLIM was also used to investigate the effects of ligand binding on the AMPA receptor intracellular domain and revealed structural changes during receptor activation [53]. All these examples show that this approach has broad applicability in neuroscience research.

FRET-FLIM has been an essential technique in our studies of NMDAR signaling. The spatial sensitivity of FRET and the fact that FLIM is not affected by factors such as fluorophore concentration make it broadly applicable to studying protein-protein interactions. Application of the FRET-FLIM technique in the study of other ionotropic receptors, such as the kainate receptor [54], could prove beneficial in expanding our understanding of the potential metabotropic functions of these receptors. We hope this guide will be helpful in addressing the methodology needed to apply this technique in future studies.

5 Notes

1. For each preparation, we freshly dissolved 6 mg of papain in 600 μ L of a saline solution (150 mM NaCl). After complete dissolution, this was added to the dissociation media.
2. The lifetime of fluorescent molecules is in the nanosecond timescale. Thus, the light source used for excitation must be able to emit pulses on a picosecond scale or shorter. In our

experiments, we are using a two-photon Chameleon Ultra II IR laser (Coherent) (80-MHz repetition rate, 100- to 150-fs pulses) tuned to 930 nm to excite GFP. However, laser diodes with pulse durations in the picosecond range are available on the market for a fraction of the price of a two-photon laser and should also work for excitation of fluorophores.

3. Both Becker & Hickl GmbH and PicoQuant GmbH, the two main companies providing FLIM instrumentation, are selling full kits for upgrading multiphoton microscopes of most brands for FLIM. Ferreira et al., who conducted similar FRET-FLIM experiments, used an alternative FLIM setup. They used a 3 W 478 nm LED (light-emitting diode) modulated at 36 MHz as an excitation source and a CCD LI2CAM camera from Lambert Instruments and the complementary LI-FLIM software [10].
4. This solution is meant to reduce ion flux through the NMDAR by increasing magnesium block. Different proportions of calcium and magnesium could be used. For 500 mL of solution, use 447.7 mL H₂O, 43.5 mL HBSS 10×, 5 mL Na-HEPES (1 M stock), 1 mL glucose solution (1 M stock), 0.3 mL CaCl₂ (1 M stock), and 2.5 mL MgCl₂ (1 M stock).
5. Neurons should be allowed to equilibrate in the imaging solution before imaging. Even when using a weight to secure the coverslip at the bottom of the perfusion chamber, there is a risk that the coverslip may move while being scanned, making stored coordinates unusable, so experimenters may choose to image neurons as they are found rather than locating all neurons suitable for imaging first. As long as adequate time for equilibration (about 10 min) is allowed before imaging begins, both methods should be equally successful.
6. This fast scanning speed is used to minimize photobleaching (for 512 × 512 pictures, it leads to an acquisition time of 0.8 s for each frame), so FLIM images are obtained from accumulating several scans together.
7. Ideally, the CFD, TAC, and ADC should be in the range of 10³ photons/s or higher while acquiring to ensure high-quality images.
8. For the purposes of our experiments, the matrices of chi-square values, pixel intensities, and color-coded values were exported into and compiled in a custom Matlab program, which allowed more convenient ROI selection and data filtration. This process can also be done in SPCImage using crosshair selection to individually find these values for each ROI but may be more painstaking. The custom Matlab program is available upon request.

References

- Collingridge G (1987) Synaptic plasticity. The role of NMDA receptors in learning and memory. *Nature* 330(6149):604–605. <https://doi.org/10.1038/330604a0>
- Riedel G, Platt B, Micheau J (2003) Glutamate receptor function in learning and memory. *Behav Brain Res* 140(1–2):1–47. [https://doi.org/10.1016/s0166-4328\(02\)00272-3](https://doi.org/10.1016/s0166-4328(02)00272-3)
- Dore K, Labrecque S, Tardif C, De Koninck P (2014) FRET-FLIM investigation of PSD95-NMDA receptor interaction in dendritic spines; control by calpain, CaMKII and Src family kinase. *PLoS One* 9(11):e112170. <https://doi.org/10.1371/journal.pone.0112170>
- Brocher S, Artola A, Singer W (1992) Intracellular injection of Ca²⁺ chelators blocks induction of long-term depression in rat visual cortex. *Proc Natl Acad Sci U S A* 89(1):123–127
- Malenka RC (1994) Synaptic plasticity in the hippocampus: LTP and LTD. *Cell Rev* 78(4):535–538
- Dore K, Aow J, Malinow R (2015) Agonist binding to the NMDA receptor drives movement of its cytoplasmic domain without ion flow. *Proc Natl Acad Sci U S A* 112(47):14705–14710. <https://doi.org/10.1073/pnas.1520023112>
- Dore K, Aow J, Malinow R (2016) The emergence of NMDA receptor metabotropic function: insights from imaging. *Front Synap Neurosci* 8:20. <https://doi.org/10.3389/fnsyn.2016.00020>
- Aow J, Dore K, Malinow R (2015) Conformational signaling required for synaptic plasticity by the NMDA receptor complex. *Proc Natl Acad Sci U S A* 112(47):14711–14716. <https://doi.org/10.1073/pnas.1520029112>
- Carter BC, Jahr CE (2016) Postsynaptic, not presynaptic NMDA receptors are required for spike-timing-dependent LTD induction. *Nat Neurosci*. <https://doi.org/10.1038/nn.4343>
- Ferreira JS et al (2017) Co-agonists differentially tune GluN2B-NMDA receptor trafficking at hippocampal synapses. *elife* 6. <https://doi.org/10.7554/eLife.25492>
- Nabavi S, Kessels HW, Alfonso S, Aow J, Fox R, Malinow R (2013) Metabotropic NMDA receptor function is required for NMDA receptor-dependent long-term depression. *Proc Natl Acad Sci U S A* 110(10):4027–4032. <https://doi.org/10.1073/pnas.1219454110>
- Wong JM, Gray JA (2018) Long-term depression is independent of GluN2 subunit composition. *J Neurosci* 38(19):4462–4470. <https://doi.org/10.1523/JNEUROSCI.0394-18.2018>
- Mayford M, Wang J, Kandel ER, O'Dell TJ (1995) CaMKII regulates the frequency-response function of hippocampal synapses for the production of both LTD and LTP. *Cell* 81(6):891–904
- Scanziani M, Malenka RC, Nicoll RA (1996) Role of intercellular interactions in heterosynaptic long-term depression. *Nature* 380(6573):446–450. <https://doi.org/10.1038/380446a0>
- Dore K, Malinow R (2021) Elevated PSD-95 blocks ion-flux independent LTD: a potential new role for PSD-95 in synaptic plasticity. *Neuroscience* 456:43–49. <https://doi.org/10.1016/j.neuroscience.2020.02.020>
- Gray NW, Weimer RM, Bureau I, Svoboda K (2006) Rapid redistribution of synaptic PSD-95 in the neocortex in vivo. *PLoS Biol* 4(11):e370. <https://doi.org/10.1371/journal.pbio.0040370>
- Zhou Q, Homma KJ, Poo MM (2004) Shrinkage of dendritic spines associated with long-term depression of hippocampal synapses. *Neuron* 44(5):749–757. <https://doi.org/10.1016/j.neuron.2004.11.011>
- Stein IS, Gray JA, Zito K (2015) Non-ionotropic NMDA receptor signaling drives activity-induced dendritic spine shrinkage. *J Neurosci* 35(35):12303–12308. <https://doi.org/10.1523/JNEUROSCI.4289-14.2015>
- Birnbaum JH, Bali J, Rajendran L, Nitsch RM, Tackenberg C (2015) Calcium flux-independent NMDA receptor activity is required for A beta oligomer-induced synaptic loss. *Cell Death Dis* 6:ARTN e1791. <https://doi.org/10.1038/cddis.2015.160>
- Dore K et al (2021) PSD-95 protects synapses from beta-amyloid. *Cell Rep* 35(9):109194. <https://doi.org/10.1016/j.celrep.2021.109194>
- Kessels HW, Nabavi S, Malinow R (2013) Metabotropic NMDA receptor function is required for beta-amyloid-induced synaptic depression. *Proc Natl Acad Sci U S A* 110(10):4033–8. <https://doi.org/10.1073/pnas.1219605110>
- Tamburri A, Dudilot A, Licea S, Bourgeois C, Boehm J (2013) NMDA-receptor activation

- but not ion flux is required for amyloid-beta induced synaptic depression. *PLoS One* 8(6): e65350. <https://doi.org/10.1371/journal.pone.0065350>
23. Weilinger NL et al (2016) Metabotropic NMDA receptor signaling couples Src family kinases to pannexin-1 during excitotoxicity. *Nat Neurosci* 19(3):432–442. <https://doi.org/10.1038/nn.4236>
 24. Park DK et al (2022) Reduced d-serine levels drive enhanced non-ionotropic NMDA receptor signaling and destabilization of dendritic spines in a mouse model for studying schizophrenia. *Neurobiol Dis* 170:105772. <https://doi.org/10.1016/j.nbd.2022.105772>
 25. Becker W, Bergmann A, Hink MA, König K, Benndorf K, Biskup C (2004) Fluorescence lifetime imaging by time-correlated single-photon counting. *Microsc Res Tech* 63(1): 58–66
 26. Lakowicz JR (2006) Principles of fluorescence spectroscopy, 3rd edn. Springer, p 954
 27. Hille C, Lahn M, Lohmannsroben HG, Dosche C (2009) Two-photon fluorescence lifetime imaging of intracellular chloride in cockroach salivary glands. *Photochem Photobiol Sci* 8(3):319–327. <https://doi.org/10.1039/b813797h>
 28. Yasuda R (2006) Imaging spatiotemporal dynamics of neuronal signaling using fluorescence resonance energy transfer and fluorescence lifetime imaging microscopy. *Curr Opin Neurobiol* 16(5):551–561
 29. Gustiananda M, Liggins JR, Cummins PL, Gready JE (2004) Conformation of prion protein repeat peptides probed by FRET measurements and molecular dynamics simulations. *Biophys J* 86(4):2467–2483. [https://doi.org/10.1016/S0006-3495\(04\)74303-9](https://doi.org/10.1016/S0006-3495(04)74303-9)
 30. Piston DW, Kremers GJ (2007) Fluorescent protein FRET: the good, the bad and the ugly. *Trends Biochem Sci* 32(9):407–414. <https://doi.org/10.1016/j.tibs.2007.08.003>
 31. Selvin PR (2000) The renaissance of fluorescence resonance energy transfer. *Nat Struct Biol, Research Support* 7(9):730–734. <https://doi.org/10.1038/78948>
 32. Sapkota K et al (2019) The NMDA receptor intracellular C-terminal domains reciprocally interact with allosteric modulators. *Biochem Pharmacol* 159:140–153. <https://doi.org/10.1016/j.bcp.2018.11.018>
 33. Kornau HC, Schenker LT, Kennedy MB, Seeburg PH (1995) Domain interaction between NMDA receptor subunits and the postsynaptic density protein PSD-95. *Science* 269(5231): 1737–1740
 34. Mulkey RM, Herron CE, Malenka RC (1993) An essential role for protein phosphatases in hippocampal long-term depression. *Science* 261(5124):1051–1055
 35. Westphal RS et al (1999) Regulation of NMDA receptors by an associated phosphatase-kinase signaling complex. *Science* 285(5424):93–96
 36. Malenka RC et al (1989) An essential role for postsynaptic calmodulin and protein kinase activity in long-term potentiation. *Nature* 340(6234):554–557. <https://doi.org/10.1038/340554a0>
 37. Malinow R, Schulman H, Tsien RW (1989) Inhibition of postsynaptic PKC or CaMKII blocks induction but not expression of LTP. *Science* 245(4920):862–866
 38. Coultrap SJ et al (2014) Autonomous CaMKII mediates both LTP and LTD using a mechanism for differential substrate site selection. *Cell Rep* 6(3):431–437. <https://doi.org/10.1016/j.celrep.2014.01.005>
 39. Bayer KU, De Koninck P, Leonard AS, Hell JW, Schulman H (2001) Interaction with the NMDA receptor locks CaMKII in an active conformation. *Nature* 411(6839):801–805. <https://doi.org/10.1038/35081080>
 40. Lee SJ, Escobedo-Lozoya Y, Szatmari EM, Yasuda R (2009) Activation of CaMKII in single dendritic spines during long-term potentiation. *Nature* 458(7236):299–304
 41. Koushik SV, Vogel SS (2008) Energy migration alters the fluorescence lifetime of Cerulean: implications for fluorescence lifetime imaging Forster resonance energy transfer measurements. *J Biomed Opt* 13(3):031204. <https://doi.org/10.1117/1.2940367>
 42. Joosen L, Hink MA, Gadella TW Jr, Goedhart J (2014) Effect of fixation procedures on the fluorescence lifetimes of Aequorea victoria derived fluorescent proteins. *J Microsc* 256(3):166–176. <https://doi.org/10.1111/jmi.12168>
 43. Tang S, Yasuda R (2017) Imaging ERK and PKA activation in single dendritic spines during structural plasticity. *Neuron* 93(6):1315–1324 e3. <https://doi.org/10.1016/j.neuron.2017.02.032>
 44. Oliveira AF, Yasuda R (2013) An improved Ras sensor for highly sensitive and quantitative FRET-FLIM imaging. *PLoS One* 8(1): e52874. <https://doi.org/10.1371/journal.pone.0052874>
 45. Murakoshi H, Wang H, Yasuda R (2011) Local, persistent activation of Rho GTPases during plasticity of single dendritic spines. *Nature* 472(7341):100–104. <https://doi.org/10.1038/nature09823>

46. Laviv T et al (2020) In vivo imaging of the coupling between neuronal and CREB activity in the mouse brain. *Neuron* 105(5):799–812 e5. <https://doi.org/10.1016/j.neuron.2019.11.028>
47. Jongbloets BC, Ma L, Mao T, Zhong H (2019) Visualizing protein kinase A activity in head-fixed behaving mice using in vivo two-photon fluorescence lifetime imaging microscopy. *J Vis Exp* 148. <https://doi.org/10.3791/59526>
48. Lodder B, Lee SJ, Sabatini BL (2021) Real-time, in vivo measurement of protein kinase a activity in deep brain structures using Fluorescence Lifetime Photometry (FLiP). *Curr Protoc* 1(10):e265. <https://doi.org/10.1002/cpz1.265>
49. Takahashi N et al (2015) Two-photon fluorescence lifetime imaging of primed SNARE complexes in presynaptic terminals and beta cells. *Nat Commun* 6:8531. <https://doi.org/10.1038/ncomms9531>
50. Sharda N, Pengo T, Wang Z, Kandimalla KK (2020) Amyloid-beta peptides disrupt interactions between VAMP-2 and SNAP-25 in neuronal cells as determined by FRET/FLIM. *J Alzheimers Dis* 77(1):423–435. <https://doi.org/10.3233/JAD-200065>
51. Marquer C et al (2011) Local cholesterol increase triggers amyloid precursor protein-Bace1 clustering in lipid rafts and rapid endocytosis. *FASEB J* 25(4):1295–1305. <https://doi.org/10.1096/fj.10-168633>
52. Winslow AR et al (2014) Convergence of pathology in dementia with Lewy bodies and Alzheimer’s disease: a role for the novel interaction of alpha-synuclein and presenilin 1 in disease. *Brain* 137(Pt 7):1958–1970. <https://doi.org/10.1093/brain/awu119>
53. Zachariassen LG, Katchan L, Jensen AG, Pickering DS, Plested AJ, Kristensen AS (2016) Structural rearrangement of the intracellular domains during AMPA receptor activation. *Proc Natl Acad Sci U S A* 113(27):E3950–E3959. <https://doi.org/10.1073/pnas.1601747113>
54. Rodriguez-Moreno A, Sihra TS (2007) Metabotropic actions of kainate receptors in the CNS. *J Neurochem* 103(6):2121–2135. <https://doi.org/10.1111/j.1471-4159.2007.04924.x>